Journal of the Ceramic Society of Japan 121 [8] 589-592 2013 Paper

Effect of sintering condition and V-doping on the piezoelectric properties of $BaTiO_3$–$Bi(Mg_{1/2}Ti_{1/2})O_3$–$BiFeO_3$ ceramics

Ichiro FUJII,† Ryuta MITSUI, Kouichi NAKASHIMA, Nobuhiro KUMADA, Hisato YABUTA,* Mikio SHIMADA,* Takayuki WATANABE,* Kaoru MIURA* and Satoshi WADA

Interdisciplinary Graduate School of Medical and Engineering, University of Yamanashi, Kofu 400–8510, Japan
***Corporate R&D Headquarters, CANON Inc., Ota, Tokyo 146–8501, Japan**

$0.3BaTiO_3$–$0.1Bi(Mg_{1/2}Ti_{1/2})O_3$–$0.6BiFeO_3$ ceramics were either doped with vanadium or sintered in calcined powder with the same composition. Compared to an undoped ceramic sintered without the calcined powder, both ceramics showed reduced leakage current densities (lower than 1×10^{-7} A/cm^2) and absence of dielectric relaxation behaviors observed in frequency- and temperature-dependent dielectric measurements. The Curie temperatures of both samples were higher than 460°C. The maximum field-induced strain over the applied field, S_{max}/E_{max}, of 366 pm/V for the undoped ceramic sintered without the calcined powder increased to 455 and 799 pm/V for the V-doped sample and the sample sintered with the calcined powder, respectively. The increase was discussed with reduced concentrations of bismuth vacancy–oxygen vacancy defect dipoles.

Key-words : Barium titanate, Bismuth magnesium titanate, Bismuth ferrite, Ferroelectric, Piezoelectric

[Received March 15, 2013; Accepted April 22, 2013]

1. Introduction

$Pb(Zr,Ti)O_3$ (PZT) has been used for electromechanical applications owing to the large piezoelectric properties over a wide temperature range.[1] Lead is, however, a toxic element, and therefore lead-free piezoelectrics have extensively been studied.[2)–12)] To date, no piezoelectric material with the piezoelectric response and Curie temperature simultaneously comparable to those of PZT was found.[13]

The large piezoelectric responses of PZT are attributed to the morphotropic phase boundary (MPB), which separates tetragonal and rhombohedral phases. There are several reported studies to understand the origin of the large response at MPB. A theoretical study explained that the increased response was attributed to increased numbers of polarizable directions as a result of coexistence of the two phases.[14] Recent transmission electron microscopy studies showed nano-sized, fine domains at MPB.[15] The motion of the fine domains by the electric field was observed, which was suggested to lead the large piezoelectric properties.[16] Since nano-sized domains are also reported for solid-solutions of relaxors $Pb(Zn_{1/3}Nb_{2/3})O_3$ and $Pb(Mg_{1/3}Nb_{2/3})O_3$ and ferroelectric $PbTiO_3$ with large piezoelectric properties,[17),18)] they may be associated with the increased piezoelectric response of PZT at MPB.

Microstructure and electric properties have been studied for lead-free piezoelectric solid-solutions of relaxor-like $(1-x)$-$BaTiO_3$–xBi$(Mg_{1/2}Ti_{1/2})O_3$ (BT–BMT) with the dielectric maximum temperature maximized to 360°C at $x = 0.5$[19),20)] and ferroelectric $BiFeO_3$ (BF) with the Curie temperature of ~830°C.[21] An early work showed nanodomains in the BT–BMT–BF system.[22),23)] The domain structure of the 0.3BT–0.1BMT–0.6BF ceramics mainly consisted of nanodomains with a small amount of large, ferroelectric domains (macrodomains).[22] The dielectric displacement–electric field loop was ferroelectric, but the loop appeared round and leaky. When the sample was doped with an acceptor of Mn, the lossy response was suppressed. However, the piezoelectric and dielectric properties were also reduced.[24]

The aim of this study is to develop 0.3BT–0.1BMT–0.6BF ceramics with reduced leakage current and without sacrificing the properties. To this end, effect of donor doping and sintering condition was investigated. Donor doping is known to increase the resistivity of Bi-based ferroelectrics of $Bi_4Ti_3O_{12}$,[25),26)] and vanadium[27] was selected in this study. Sintering a Bi-based sample in a bismuth-rich atmosphere would suppress Bi_2O_3 evaporation, as reported for a lead-based system.[28] To determine if this is true for the 0.3BT–0.1BMT–0.6BF ceramics, the compacts were sintered either in a closed crucible fully filled with the calcined powder with the same composition or in a closed, empty crucible.

2. Experimental procedure

Three different samples were studied: undoped 0.3BT–0.1BMT–0.6BF ceramics sintered in a closed crucible without a cover calcined powder with the same composition (undoped sample), undoped 0.3BT–0.1BMT–0.6BF ceramics sintered in a closed crucible fully filled with the cover calcined powder (embedded sample), and V-doped ceramics with the composition of $0.3BT–0.1Bi_{1-y/6}[Mg_{1/2}Ti_{(1-y)/2}V_{y/2}]O_3$–0.6BF with $y = 0.02$ sintered in the closed crucible without the cover calcined powder (V-doped sample). The crucible was made of Al_2O_3 (99%) with a size of ϕ36 mm × 30 mm. A lid made of the same alumina was placed on the crucible. The samples were prepared by a solid-state synthesis. Powders of $BaTiO_3$ (Sakai Chemical, BT01), Bi_2O_3 (99.999%, Rare Metallic), MgO (99.9%, Rare Metallic), TiO_2 (Ishihara Sangyo, MPT-851), α-Fe_2O_3 (99.99%, Rare Metallic), and V_2O_5 (99.0%, Kanto Chemical) were weighed and ball-milled with zirconia balls and ethanol for 16 h. After drying at 80°C, the powders were ground and calcined at 800°C for 6 h in a closed crucible. The calcined powders were again ground, and then the crystal structures were examined by X-ray

† Corresponding author: I. Fujii; E-mail: ifujii@rins.ryukoku.ac.jp

DOI http://dx.doi.org/10.2109/jcersj2.121.589

diffraction (XRD; Rigaku, RINT2000) with Cu Kα radiation. They were again ball-milled for 16 h, followed by drying. After adding a binder, the powders were uniaxially pressed at 250 MPa to disc compacts. The binder was removed at 600°C. The compacts were sintered at 1000°C for 2 h at a heating rate of 300°C/h in the crucible with or without the calcined powder. The densities of the samples were measured by an Archimedes method. For crystal structure characterization, polished surfaces of the sintered samples were examined by the XRD analysis.

For electric characterizations, the samples were polished down to 0.4 mm in thickness. Gold electrodes were formed on both surfaces by sputtering, and the samples were heated at 300°C for 10 min to improve the adhesion. The samples were sawed into a size of $4 \times 1.5 \times 0.4\,mm^3$. The room temperature dielectric constant and loss were measured at frequencies from 40 Hz to 1 MHz using an impedance analyzer (HP4294A, Agilent). Temperature dependence of the dielectric properties was measured at 10, 100 kHz, and 1 MHz using an LCR meter (6440B, Wayne Kerr Electronics), with increasing temperature from room temperature to 500–550°C at a heating rate of 3°C/min. The dielectric displacement–electric field loops were measured by a ferroelectric characteristics evaluation system (FCE-3, Toyo Corporation). The strain–electric field curves were measured using a strain measuring system (Model JP005-SE, Kitamoto Denshi) with a displacement meter (Millitron 1202 IC, Mahr).

3. Results and discussion

3.1 Physical and structural properties

Figure 1 shows the XRD patterns of the sintered samples. Only the perovskite phase was observed. The crystal structures of all the samples were pseudo-cubic, and this was consistent with previous studies.[22),24)] The pseudo-cubic lattice parameter was calculated by a least-square fit of selected XRD peaks. The pseudo-cubic lattice parameter for the samples was $3.997(8) \pm 0.000(3)$ Å and did not change among the samples. Here, the lattice constant of the V-doped sample was the same as that of the undoped and embedded samples, probably because the amount of the V dopant was small, which was consistent with previous study.[27)] The densities of the samples were 95–96% of the theoretical values.

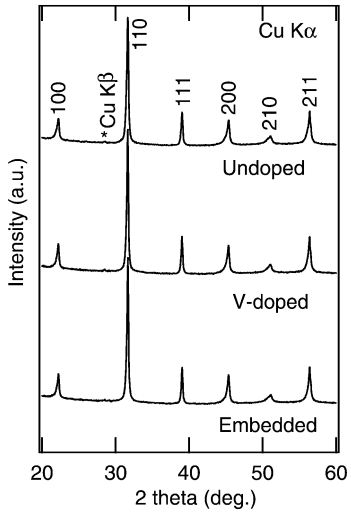

Fig. 1. The XRD patterns of the undoped, V-doped, and embedded samples.

3.2 Leakage and dielectric properties

The leakage current density–electric field response is shown in **Fig. 2**. The leakage current density of the undoped sample increased to $10^{-6}\,A/cm^2$ at 40 kV/cm. Beyond the electric field, the sample was broken down. A large leakage current density has been reported for Bi-based materials.[27),29),30)] When the undoped sample was embedded or V-doped, the leakage current density was reduced to 10^{-9}–$10^{-8}\,A/cm^2$. The reduction in the leakage current density of the embedded sample was attributed to the suppression of Bi_2O_3 evaporation. The Bi_2O_3 evaporation in the undoped sample might lose a local electrical neutrality,[31)] which resulted in a change in an oxidation state of Fe ions between Fe^{3+} and Fe^{2+}. The change in the oxidation state is known to lead a hopping conduction between the Fe ions and increased the leakage current density.[29),30)] For the V-doped sample, bismuth vacancies were generated, that is, $Bi_{1-x/6}[Mg_{1/2}Ti_{(1-x)/2}V_{x/2}]O_3$. This could inhibit a further generation of bismuth vacancies as well as oxygen vacancies, which reduced the leakage current density, as proposed for V-doped $Bi_4Ti_3O_{12}$.[27)]

The frequency dependence of the dielectric properties is shown in **Fig. 3**. A clear increase in the dielectric loss at low frequencies was observed for the undoped sample. This increase could be ascribed to an electric conduction and/or a dielectric relaxation which was either a migration of space charges or a reorientation of defect dipoles.[32)] For the undoped sample, a concentration of the oxygen vacancies could be high due to the Bi_2O_3 evaporation. As reported for other perovskite oxides,[33),34)] these oxygen vacancies could migrate as space charges or move around bismuth vacancies, resulted in bismuth vacancy–oxygen vacancy defect dipoles. When the sample was sintered with the calcined powder or doped with V, the increase in the dielectric loss was suppressed.

The temperature dependence of the dielectric properties is shown in **Fig. 4**. For the dielectric constant profile of the undoped sample, there are two peaks observed. One is the peak

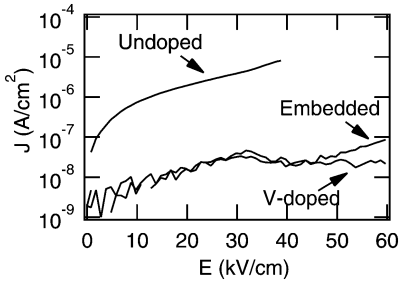

Fig. 2. The room temperature leakage current density–electric field (J–E) response of the undoped, V-doped, and embedded samples.

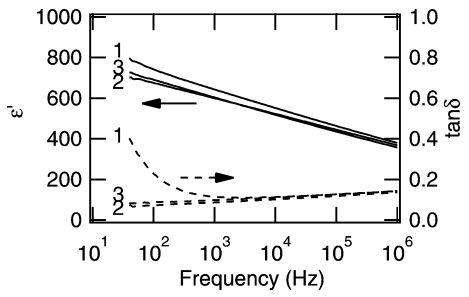

Fig. 3. The frequency dependence of the room temperature dielectric constant, ε', and dielectric loss, $\tan\delta$, of (1) undoped, (2) V-doped, and (3) embedded samples.

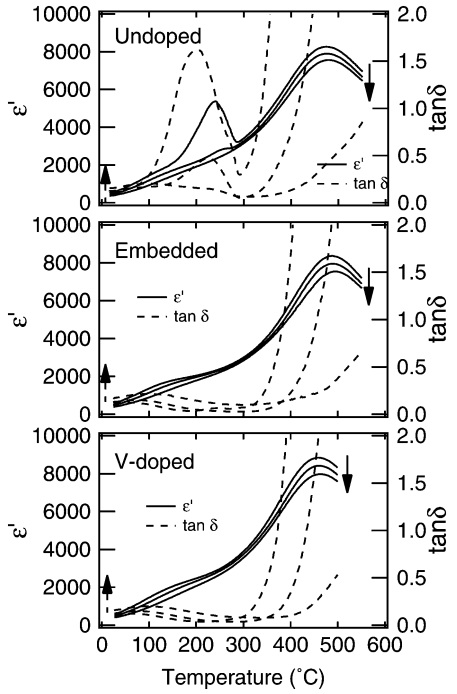

Fig. 4. The temperature dependence of the dielectric constant, ε', and dielectric loss, tan δ, measured at the frequencies of 10, 100 kHz, and 1 MHz. The arrows indicate the direction of increasing frequency.

at 480°C, which is associated with the Curie temperature.[22] The peak dielectric constant decreased with increasing frequency. This was related to an electric conduction, as evidenced by the large increase in the dielectric loss at high temperatures. The other is the peak with a strong frequency dependence near 230°C, accompanied with the dielectric loss peak. Such a peak is related to the dielectric relaxation,[33),34)] and thus this supports that the dielectric loss increase observed in Fig. 3 was, at least, associated with the dielectric relaxation. For the sample doped with V or sintered in the calcined powder, the peak near 230°C was suppressed. The leakage and dielectric data suggest that there were a large concentration of the defect dipoles and/or space charges in the undoped sample. These defects might connect to form leakage paths, and thus result in the large leakage current density. For the V-doped and embedded samples, the defect concentrations were reduced. The defects were isolated and did not form the leakage paths, leading to the reduced leakage.

The Curie temperature was reduced by 20°C for the V-doped sample. A reduction in the Curie temperature by V-doping was reported for $Bi_4Ti_3O_{12}$ ceramics, although the reduction was smaller.[27)] On the other hand, the Curie temperature was raised by 15°C for the embedded sample. A possible reason for this is the reduced oxygen vacancy concentration, as reported for $BaTiO_3$.[35)]

At temperatures between room temperature and 200°C, a frequency dispersion in the dielectric constant and loss was observed for the V-doped sample and the embedded sample. A similar dispersion was found in BT–BF and BT–$BiScO_3$ solid solutions,[36),37)] and therefore this could be a characteristic of $BaTiO_3$–Bi-based perovskite systems. The origin was suggested to be reentrant, which meant that the material could be treated as dipolar glass.[36)]

3.3 Ferroelectric and piezoelectric properties

The dielectric displacement–electric field loops of the samples are shown in **Fig. 5**. A leaky, round loop was observed for the

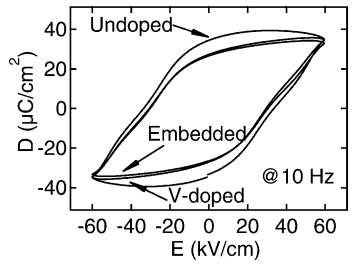

Fig. 5. The dielectric displacement–electric field (D–E) loops of the undoped, V-doped, and embedded samples, measured at 10 Hz.

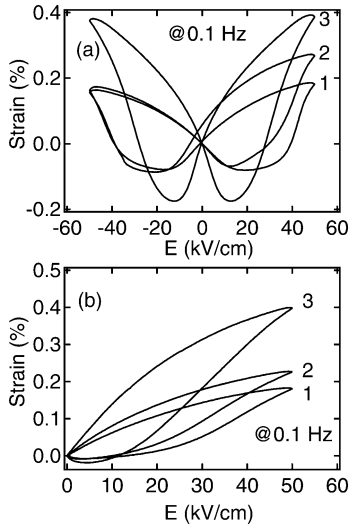

Fig. 6. (a) The bipolar and (b) unipolar strain–electric field curves of (1) undoped, (2) V-doped, and (3) embedded samples, measured at 0.1 Hz. The samples were not poled.

undoped sample. This was at least associated with the increased leakage current density presented in Fig. 2. The space charges, as suggested in the frequency and temperature studies, could contribute to this as well. The hysteresis loop was slightly pinched. Pinched hysteresis loops were reported for ferroelectrics including BF,[38)–41)] and were attributed to defect dipoles. For the embedded sample and the V-doped sample, such a lossy response was suppressed. No large difference was observed for the loops. Note that the hysteresis loops were also slightly pinched, suggesting a small amount of the defect dipoles that was not detected by the tan δ–frequency response.

The bipolar strain–electric field curves of the samples are shown in **Fig. 6**(a). It was found that the field-induced strain was increased for the embedded and V-doped samples, compared to the undoped sample. This could be attributed to the reduced concentrations of the defect dipoles that pinned the domain wall motion. The asymmetric curve was observed for the V-doped sample. Such a curve was reported for a $BiFeO_3$ ceramic.[42)] Note that the coercive field was smaller than those of the dielectric displacement–electric field loops because of the lower measuring frequencies. With increasing frequency, a coercive field of a ferroelectric increases due to a delayed response of domain walls with respect to the applied electric field,[43)] and the frequency dependence was mainly attributed to a slow response of a non-180° domain wall motion.[42),44)] Recent studies showed the strong frequency dependence of the coercive field in $0.7Pb(Mg_{1/3}Nb_{2/3})O_3$–$0.3PbTiO_3$ and $0.955Pb(Mg_{1/3}Nb_{2/3})O_3$–$0.045PbTiO_3$ systems with compositions having nanodomains.[45),46)] These might

suggest that the strong frequency dependence of the coercive field of the samples in this study was associated with an increased concentration of non-180° domain walls due to their nano-domains. The unipolar strain–electric field curves of the samples are shown in Fig. 6(b). Note that the samples were not poled. As expected, increased responses were observed for the embedded sample and the V-doped sample. The strain maximum/applied electric field amplitude, S_{max}/E_{max}, at $E_{max} = 50\,kV/cm$, 0.1 Hz, was 366, 799, and 455 pm/V for the undoped sample, the embedded sample, and the V-doped sample, respectively. These results indicated that the sintering with the calcined powder and the V-doping (especially the embedded case) were effective in increasing large-field piezoelectric response, possibly due to reduced defect dipole concentrations. The origin of the smaller strain response of the V-doped sample compared to that of the embedded sample is unclear and needs further study.

4. Conclusions

The leakage, dielectric, and piezoelectric properties of the undoped, embedded, and V-doped samples were studied. The large current densities and the dielectric relaxation of the undoped sample were suppressed for the embedded sample and the V-doped sample. The electric-field-induced strain was increased for the embedded and V-doped samples. The dielectric relaxation and the pinched P-E loops suggested that the increase was associated with the reduced concentrations of the defect dipoles.

Acknowledgements The authors would like to thank Sakai Chemical Industry Co., Ltd., for providing $BaTiO_3$ powders. This study was supported by Elements Science and Technology Project of the Ministry of Education, Culture, Sports, Science and Technology, Japan.

References

1) B. Jaffe, W. R. Cook and H. L. Jaffe, "Piezoelectric ceramics", Academic Press, New York (1971).
2) Y. Saito, H. Takao, T. Tani, T. Nonoyama, K. Takatori, T. Homma, T. Nagaya and M. Nakamura, *Nature*, **432**, 84–87 (2004).
3) K. I. Kakimoto, T. Imura, Y. Fukui, M. Kuno, K. Yamagiwa, T. Mitsuoka and K. Ohbayashi, *Jpn. J. Appl. Phys.*, **46**, 7089–7093 (2007).
4) E. Z. Li, H. Kakemoto, T. Hoshina and T. Tsurumi, *Jpn. J. Appl. Phys.*, **47**, 7702–7706 (2008).
5) Y. Hiruma, T. Watanabe, H. Nagata and T. Takenaka, *Jpn. J. Appl. Phys.*, **47**, 7659–7663 (2008).
6) Y. Isikawa, Y. Akiyama and T. Hayashi, *Jpn. J. Appl. Phys.*, **48**, 09KD03 (2009).
7) S. Yasui, O. Sakata, M. Nakajima, S. Utsugi, K. Yazawa, T. Yamada and H. Funakubo, *Jpn. J. Appl. Phys.*, **48**, 09KD06 (2009).
8) M. Suzuki, A. Morishita, Y. Kitanaka, Y. Noguchi and M. Miyayama, *Jpn. J. Appl. Phys.*, **49**, 09MD09 (2010).
9) H. Nagata, M. Saitoh, Y. Hiruma and T. Takenaka, *Jpn. J. Appl. Phys.*, **49**, 09MD08 (2010).
10) Y. Doshida, H. Shimizu, Y. Mizuno, K. Itoh, S. Hirose and H. Tamura, *Jpn. J. Appl. Phys.*, **50**, 09ND06 (2011).
11) M. Kobune, K. Teraoka, H. Nishioka, H. Yamaguchi and K. Honda, *Jpn. J. Appl. Phys.*, **50**, 09ND08 (2011).
12) T. Watanabe, M. Shimada, T. Aiba, H. Yabuta, K. Miura, K. Oka, M. Azuma, S. Wada and N. Kumada, *Jpn. J. Appl. Phys.*, **50**, 09ND01 (2011).
13) T. R. Shrout and S. J. Zhang, *J. Electroceram.*, **19**, 111–124 (2007).
14) W. W. Cao and L. E. Cross, *Phys. Rev. B*, **47**, 4825–4830 (1993).
15) K. A. Schönau, L. A. Schmitt, M. Knapp, H. Fuess, R. d.-A. Eichel, H. Kungl and M. J. Hoffmann, *Phys. Rev. B*, **75**, 184117 (2007).
16) R. Theissmann, L. A. Schmitt, J. Kling, R. Schierholz, K. A. Schonau, H. Fuess, M. Knapp, H. Kungl and M. J. Hoffmann, *J. Appl. Phys.*, **102**, 024111 (2007).
17) I. K. Bdikin, V. V. Shvartsman and A. L. Kholkin, *Appl. Phys. Lett.*, **83**, 4232–4234 (2003).
18) D. Viehland, M. C. Kim, Z. Xu and J. F. Li, *Appl. Phys. Lett.*, **67**, 2471–2473 (1995).
19) S. Wada, K. Yamato, P. Pulpan, N. Kumada, B. Y. Lee, T. Iijima, C. Moriyoshi and Y. Kuroiwa, *J. Appl. Phys.*, **108**, 094114 (2010).
20) I. Fujii, K. Yamato, M. Shimada, J. Hayashi, H. Yabuta, M. Kubota, K. Nakashima, N. Kumada and S. Wada, *Key Eng. Mater.*, **485**, 31–34 (2011).
21) M. M. Kumar, V. R. Palkar, K. Srinivas and S. V. Suryanarayana, *Appl. Phys. Lett.*, **76**, 2764–2766 (2000).
22) R. Mitsui, I. Fujii, K. Nakashima, N. Kumada, Y. Kuroiwa and S. Wada, *Ceram. Int.*, **39**, S695–S699 (2013).
23) H. Yabuta, M. Shimada, T. Watanabe, J. Hayashi, M. Kubota, K. Miura, T. Fukui, I. Fujii and S. Wada, *Jpn. J. Appl. Phys.*, **51**, 09LD04 (2012).
24) I. Fujii, R. Mitsui, K. Nakashima, N. Kumada, M. Shimada, T. Watanabe, J. Hayashi, H. Yabuta, M. Kubota, T. Fukui and S. Wada, *Jpn. J. Appl. Phys.*, **50**, 09ND07 (2011).
25) H. S. Shulman, M. Testorf, D. Damjanovic and N. Setter, *J. Am. Ceram. Soc.*, **79**, 3124–3128 (1996).
26) S. H. Hong, S. Trolier-McKinstry and G. L. Messing, *J. Am. Ceram. Soc.*, **83**, 113–118 (2000).
27) Y. Noguchi and M. Miyayama, *Appl. Phys. Lett.*, **78**, 1903–1905 (2001).
28) G. S. Snow, *J. Am. Ceram. Soc.*, **56**, 91–96 (1973).
29) Y. P. Wang, L. Zhou, M. F. Zhang, X. Y. Chen, J. M. Liu and Z. G. Liu, *Appl. Phys. Lett.*, **84**, 1731–1733 (2004).
30) S. Hunpratub, P. Thongbai, T. Yamwong, R. Yimnirun and S. Maensiri, *Appl. Phys. Lett.*, **94**, 062904 (2009).
31) M. Maglione and M. A. Subramanian, *Appl. Phys. Lett.*, **93**, 032902 (2008).
32) A. J. Moulson and J. M. Herbert, "Electroceramics: materials, properties, applications", Wiley, Chichester (2003).
33) O. Bidault, P. Goux, M. Kchikech, M. Belkaoumi and M. Maglione, *Phys. Rev. B*, **49**, 7868–7873 (1994).
34) C. Ang, Z. Yu and L. E. Cross, *Phys. Rev. B*, **62**, 228–236 (2000).
35) S. Lee, Z. K. Liu, M. H. Kim and C. A. Randall, *J. Appl. Phys.*, **101**, 054119 (2007).
36) H. Y. Guo, C. Lei and Z.-G. Ye, *Appl. Phys. Lett.*, **92**, 172901 (2008).
37) S. O. Leontsev and R. E. Eitel, *J. Am. Ceram. Soc.*, **92**, 2957–2961 (2009).
38) H. J. Hagemann, *J. Phys. C Solid State Phys.*, **11**, 3333–3344 (1978).
39) K. Carl and K. H. Hardtl, *Ferroelectrics*, **17**, 473–486 (1978).
40) G. L. Yuan, Y. Yang and S. W. Or, *Appl. Phys. Lett.*, **91**, 122907 (2007).
41) A. Y. Kim, Y. J. Lee, J. S. Kim, S. H. Han, H. W. Kang, H. G. Lee and C. I. Cheon, *J. Korean Phys. Soc.*, **60**, 83–87 (2012).
42) T. Rojac, M. Kosec and D. Damjanovic, *J. Am. Ceram. Soc.*, **94**, 4108–4111 (2011).
43) F. Jona and G. Shirane, "Ferroelectric crystals", Macmillan, New York (1962).
44) J. E. Daniels, T. R. Finlayson, M. Davis, D. Damjanovic, A. J. Studer, M. Hoffman and J. L. Jones, *J. Appl. Phys.*, **101**, 104108 (2007).
45) D. Viehland and Y. H. Chen, *J. Appl. Phys.*, **88**, 6696–6707 (2000).
46) J. H. Yin and W. W. Cao, *Appl. Phys. Lett.*, **80**, 1043–1045 (2002).